PROCEEDINGS OF SCIENCE

# Performance of the CMS Muon System with Early Run 3 Data

## A. Sharma[*]

*RWTH, Aachen,*
*on behalf of the CMS Muon Collaboration*

*E-mail:* archie.sharma@cern.ch

A high-performance muon detector system is crucial to realise physics goals of the Compact Muon Solenoid (CMS) experiment at the Large Hadron Collider (LHC). The CMS muon spectrometer, consisting of different detector technologies across different pseudorapidity ($\eta$) regions, demonstrated efficient tracking and triggering of muons during Run 1 and Run 2 of the LHC operations. The legacy CMS muon detector system, consists of drift tube (DT) chambers in the barrel and cathode strip chambers (CSC) in the endcap region, complemented by Resistive Plate Chambers (RPC) in both the barrel and endcaps. During the long shutdown (LS) 2, Gas Electron Multiplier (GEM) chambers were added in the first station of forward region to enhance the redundancy of the muon system while maintaining the precision of muon momentum resolution at the Level-1 trigger. This document presents the performance studies for all four muon sub-detector systems, carried out using the data-sets collected at a collision energy of 13.6 TeV in 2022 and 2023, and compared with the Run 2 results.

---

[*]Speaker

## 1. Introduction

Muons are an unmistakable signature of most of the physics LHC is designed to explore. The CMS detector [1, 2] at the CERN LHC is a general purpose device and the ability to trigger on and reconstruct muons at the highest luminosities is central to the concept of CMS. The CMS muon system which uses the combination of different gaseous detector technologies and covers an angular region delimited by $|\eta|<$ 2.4, is divided in two major regions: barrel and endcap. The Drift Tubes (DT) are the part of muon barrel chambers which provide a precise measurement in the bending plane, up to $\eta$=1.2. The Cathode Strip Chambers (CSC) in endcap, up to $\eta$=2.4, provide high precision in the presence of a large and varying magnetic field, while their faster response time and finer segmentation allow them to function in the higher rate environment. The Resistive Plate Chambers (RPC) present in both barrel and endcap helps to provide a redundant and complementary trigger capability over nearly the entire rapidity range, thanks to their excellent timing resolution. The excellent performance of CMS Muon detector during Run 1 and Run 2 is described in these previous publications [3, 4]. To prepare for the higher collision energy and luminosity of the subsequent running period ("Run 3" started in 2022), significant improvements were made to the muon system in 2019–2021 during the long shutdown period between Runs 2 and 3 and, in addition, a new detector based on triple Gas Electron Multiplier (GEM) technology was introduced in the first endcap station to improve muon momentum resolution, while maintaining excellent trigger efficiency in the CMS forward region [2]. This paper describes the performance of the Run 3 CMS muon system with the p-p collision data taken during 2022-2023 and a comparison is presented with the Run 2 performance.

## 2. The CMS Muon Detector

The CMS detector has a cylindrical geometry that is azimuthally ($\phi$) symmetric with respect to the beamline and features a superconducting magnet, which provides a 3.8 T solenoidal field oriented along the beam line [1, 2]. The muon system is located outside the solenoid and covers the range $|\eta| <$ 2.4. The muon sub-detectors are sandwiched among the layers of the steel flux-return yoke that allow a traversing muon to be detected at multiple points along the track path. The barrel region segmentation follows that of the iron yoke, consisting of 5 wheels (numbered from -2 to +2) along the z-axis, each divided in to 12 azimuthal ($\phi$) sectors (Sec 1-12). Within each wheel, the DT and RPC chambers are arranged in four stations at different radii, labeled as MB1–MB4 and RB1–RB4, respectively. The DTs are segmented into drift cells; the position of the muon is determined by measuring the drift time to an anode wire of a cell with a shaped electric field. The two innermost RPC barrel stations, RB1 and RB2, are instrumented with two layers of RPCs each, while stations 3 and 4 the RPCs have only one detection layer. The RPC strips are oriented parallel to the wires of the DT chambers that measure the coordinate in the bending plane. From the readout point of view, every RPC is subdivided into two or three $\eta$ partitions called "rolls".

The two endcaps (-z and +z sides) made of 3 iron disks and 4 layers divided in 2 or 3 stations (ME1/1, ME1/2, ME1/3, ME2/1, ME2/2, ME3/1, ME3/2, ME4/1 and ME4/2) of CSC and RPC chambers. Each CSC chamber consists of six staggered layers, each of which measures the muon position in two coordinates. The cathode strips are oriented radially to measure the muon position

in the bending plane (R-$\phi$), whereas the anode wires provide a coarse measurement in R. The RPC strips are oriented parallel to the CSC strips to measure the coordinate in the bending plane, and each endcap chamber is divided into three $\eta$ partitions (rolls) identified by the letters A, B, and C. The fourth muon sub-system, GEMs were installed in the innermost endcap muon station (labeled as GE1/1 and GE-1/1) with the aim to extend tracking and trigger capabilities in the forward region, $1.6 < |\eta| < 2.4$ [5].

## 3. Performance results from early Run 3 data

On July 5, 2022, after over 3 years of shutdown, the LHC returned with a new energy world record of 13.6 trillion electron volts (13.6 TeV) in its first stable-beam collisions, called Run 3. Total integrated luminosity of 73.4 f$b^{-1}$ has been collected so far in 2022-2023 with peak luminosity reaching 2.5 x $10^{34}$ $cm^{-2}$ $s^{-1}$ and pile-up ($|\mu|$) = 52. The operation of the muon system has been smooth since the beginning of Run 3 and its contribution to the CMS downtime is below 2 %. The performance of each sub-system has been explained in details in the next subsections.

### 3.1 DT

DT has shown excellent performance in Run 3 so far with a fraction of active channels > 99 %. The active channels are the representation of cells with non-zero occupancy. Figure 1 (left) shows the Run 2 and Run 3 comparison of the summary of the percentage of active channels (1 entry per chamber). In Run 3, only 68 % of channels of the MB1 chamber of Wheel+2, Sector 5, are readout. Therefore this chamber is in underflow in the 2022 and 2023 plots, while for all other chambers, the performance in Run 3 is consistent with Run 2 (99.7%).
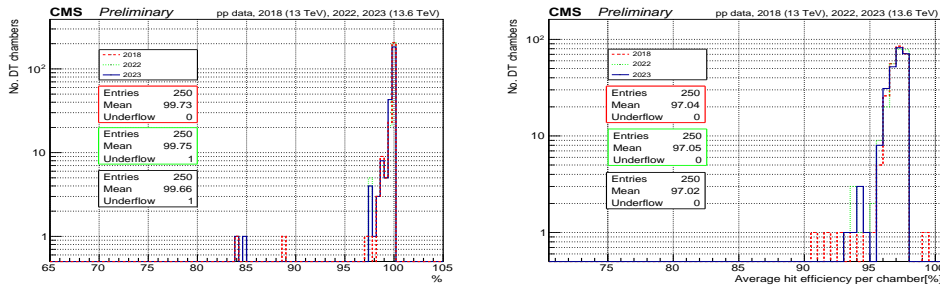


**Figure 1:** Summary of the percentage of active channels (left) and hit efficiency (right), showing the comparison of Run 2 and Run 3 performance for DT chambers.

Figure 1 (right) shows the comparison of DT hit efficiency with Run 2 and Run 3 data, where the hit efficiency is the efficiency to detect a single hit and measured as the ratio between the number of detected and expected hits described in details here [6]. Due to the known major hardware problems in the $\theta$ layers (along r-z direction) in MB1 chamber of Wheel+2, Sector 5 during Run 3 and the similar issue which appeared in MB2 chamber of Wheel+2, Sector 7 during Run 2 (in 2018 data-taking and repaired during LS2), the efficiency computed in these two cases only refers to $\phi$ layers (along r-$\phi$ direction).

Figure 2 shows the DT local segment reconstruction efficiency per chamber (left) and efficiency summary (right), defined as the efficiency to reconstruct a local track segment and measured using

a Tag & Probe method. Events were selected to contain a pair of oppositely charged reconstructed muons from Z events, more details can be find here [6]. In general, efficiency is above 99%, with few exceptions due to known hardware problems. e.g. two under-flows in the left plot reported in light blue and the efficiency is reported as text.
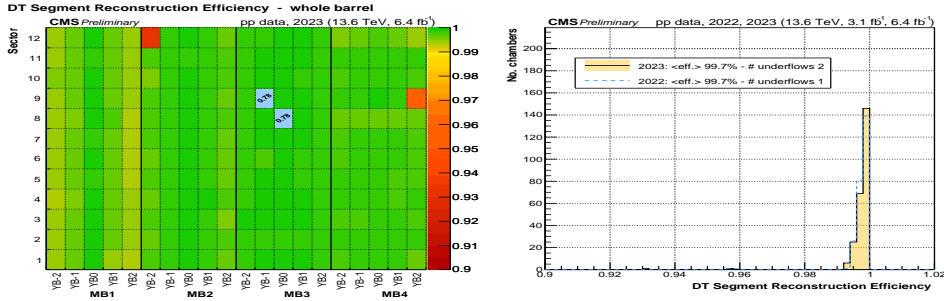


**Figure 2:** Local segment reconstruction efficiency per chamber (left) and summary (right) for 2022 and 2023 (one entry per chamber) measured with Tag & Probe using Z$\rightarrow \mu\mu$ sample.

## 3.2 CSC

CSCs are also showing an excellent and smooth performance in Run 3 for the endcap region of muons, where the magnetic field is stronger and non-uniform and higher rate of $\gamma$ and neutron induced background is expected unlike in the barrel region. Figure 3 (left) shows the global x and y position of reconstructed CSC hits in the four stations of the +z and -z endcaps of the CMS endcap muon system from one run (166 p$b^{-1}$) of a muon-triggered dataset. The reconstructed hit occupancy is generally uniform across all chambers of the same station and ring, with highest densities closer to the beam line and closer to the pp interaction point (z = 0). The regions without hits are generally understood due to some known issues, repairing time depending on the nature of the problem e.g. one chamber in ring 2 of station 4 in -z is permanently disabled because of failed electronics which cannot be accessed without opening the full CMS detector.
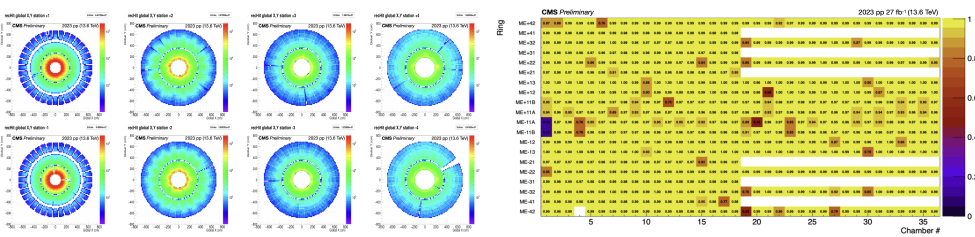


**Figure 3:** The global x and y position of reconstructed CSC hits in the four CSC stations of the +z and -z endcaps (left). The Trigger Primitive efficiency (right) of all CSC chambers, measured with Tag & Probe using Z$\rightarrow \mu\mu$ sample.

An important role of the CSC system is to supply 'Trigger Primitives' to the Level-1 muon trigger system of CMS. The CSC Trigger Primitive efficiency is defined as the ratio between number of observed trigger primitives and the expected number of trigger primitives. These efficiencies are measured with Tag & Probe technique using Z$\rightarrow \mu\mu$ sample [7], shown in Figure 3 (right). Despite few chambers showing lower efficiencies due to various known reasons, more than 98% of

the CSC system is operating at close to 100% efficiency and no significant loss in muon trigger and reconstruction efficiency is observed thanks to the highly efficient and redundant design of CSCs.

### 3.3 RPC

RPCs hit efficiencies are shown in Figure 4 for both barrel (left) and endcap (right) regions, showing the stable behaviour over time and in agreement with the expectations comparing to Run 2. Efficiencies are obtained with segment exploration method described in details here [8], using DT segments in barrel and CSC segments in endcaps. To estimate the performance of the RPC system configuration during the data taking, all RPC rolls with known hardware problems or which fall under the CMS gas leak reduction policy [9](for barrel region only) are excluded.
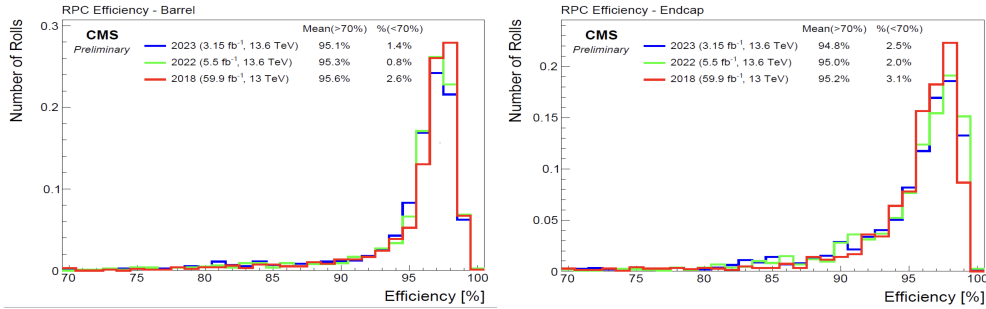


**Figure 4:** Efficiency distribution of RPC rolls in Barrel (left) and Endcap (right) obtained using the segment exploration method. Comparison is shown between Run 2 and Run 3 performances.

### 3.4 GEM

The GEM operations in the beginning of Run 3 showed the phenomenon of discharges in the presence of beam collisions, correlated to the extreme event of short circuit generation in the GEM foil. Discharges can be generated by the passage of highly ionising particles traversing the gas medium such as neutrons, and causing the breakdown of gas medium due to the presence of a big charge during the multiplication of primary ionisation electrons. After the intense monitoring and thorough study [10], HV working point was tuned to 690 $\mu$A for 2022 data-taking, stabilising the discharge rate which allowed the smooth operations of GEMs.

Figure 5 (left) shows the number of GEM's active channel fractions which is represented by fraction of active front-end chips called VFAT (Very Forward ATLAS and TOTEM) chips ([5]). Using the HV working point of 680 $\mu$A in 2023, helped to further reduce the instabilities and increase of ~10-15% in the number of active channel fraction during the cosmic/collision data-taking in 2023 compared to 2022, as well as maintaining the muon detector efficiency close to 94% for all working GEM chambers shown in Figure 5 (right).

### 4. Summary

After the excellent performance of CMS Muon system in Run 2, which played a key role for many physics results from CMS, the same performance observed in the early data-taking period of Run 3. The contribution from the muon detectors to the CMS downtime is very small and some
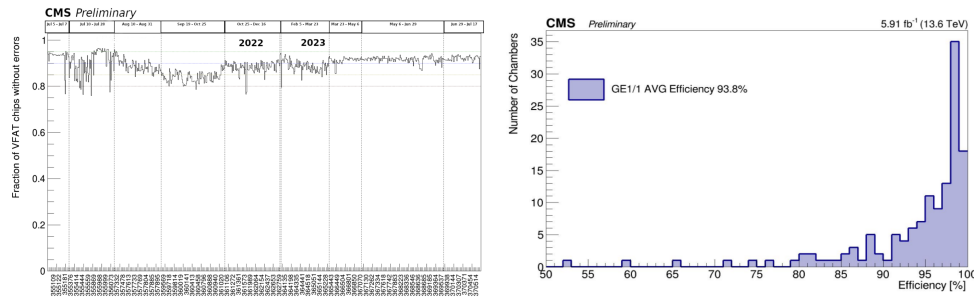
**Figure 5:** Fraction of GEM active channels represented by fraction of VFAT3 front-end chips without readout errors during stable pp collision or cosmic ray runs in 2022 and 2023 (left) and the muon detection efficiency (right) of the GEM chambers using a subset of 2023 muon dataset (5.91 fb$^{-1}$) enriched with muons from Z boson decay.

known issues, mainly occasional, and understood, don't noticeably affect the muon reconstruction efficiency, thanks to the redundant design of the muon system. Muon detection will retain its crucial role in exploring the exciting physics ahead of us.

## References

[1] CMS Collaboration, The CMS experiment at the CERN LHC, JINST 3 (2008) S08004.

[2] CMS Collaboration, Development of the CMS detector for the CERN LHC Run 3, JINST (2023), arXiv:2309.05466.

[3] CMS Collaboration, The performance of the CMS muon detector in proton-proton collisions at $\sqrt{s}$ = 7 TeV at the LHC, JINST 8 (2013) P11002.

[4] CMS Collaboration, Performance of the CMS muon detector and muon reconstruction with proton-proton collisions at $\sqrt{s}$ = 13 TeV, JINST 13 (2018) P06015.

[5] CMS Collaboration, CMS Technical Design Report for the Muon Endcap GEM Upgrade, CERN-LHCC-2015-012, CMS-TDR-013.

[6] CMS Collaboration, Performance of the CMS Drift Tubes at the end of LHC Run 2 CMS Detector Performance Note CMS-DP-2019-008, https://cds.cern.ch/record/2673608.

[7] CMS Collaboration, CSC Performance in 2017 CMS Detector Performance Note CMS-DP-2017-038.

[8] CMS Collaboration, Performance study of the CMS barrel resistive plate chambers with cosmic rays, JINST 5 (2010) T03017.

[9] Beatrice Mandelli *et al*., Strategies for reducing the use of greenhouse gases from particle detectors operation at the CERN LHC Experiments, 2022 J. Phys.: Conf. Ser. 2374 012159.

[10] S. Calzaferri on behalf of the CMS Muon Group, Study of discharges in the CMS GEM GE1/1 station with LHC beam, JINST 18 (2023) C06016.